Construction and Building Materials 400 (2023) 132806

Contents lists available at ScienceDirect

Construction and Building Materials

journal homepage: www.elsevier.com/locate/conbuildmat

Alterations in the reaction properties of Portland cement against coupled deteriorations of magnesium and sulfate upon carbonation curing☆

Joonho Seo [a,b], Naru Kim [a], Beomjoo Yang [c,*], G.M. Kim [d,e,*]

[a] Department of Civil and Environmental Engineering, Korea Advanced Institute of Science and Technology (KAIST), 291 Daehak-ro, Yuseong-gu, Daejeon 34141, Republic of Korea
[b] Applied Science Research Institute, Korea Advanced Institute of Science and Technology (KAIST), 291 Daehak-ro, Yuseong-gu, Daejeon 34141, Republic of Korea
[c] School of Civil Engineering, Chungbuk National University, 1 Chungdae-ro, Seowon-gu, Cheongju, Chungbuk 28644, Republic of Korea
[d] Mineral Processing & Metallurgy Research Center, Resources Utilization Division, Korea Institute of Geoscience and Mineral Resources, 124 Gwahak-ro, Yuseong-gu, Daejeon 34132, Republic of Korea
[e] Department of Resources Recycling, Korea University of Science and Technology, 217 Gajeong-ro Yuseong-gu, Daejeon 34113, Republic of Korea

ARTICLE INFO

Keywords:
Portland cement
Carbonation curing
$MgSO_4$
Deterioration
CO_2 sequestration

ABSTRACT

The present study explored the alterations in the reaction properties of Portland cement (PC) against coupled deteriorations of magnesium and sulfate upon carbonation curing. The physical and chemical features of the samples containing $MgSO_4$ at levels of 0, 1, 5, or 10 wt% were evaluated under the 10% carbonation curing condition for 27 days. The test results provided in this study signified that the incorporated $MgSO_4$ reduced the reaction of clinkers, thereby reducing the compressive strength development of the samples, still the strength was vastly enhanced by the carbonation curing. The carbonation curing resulted in the presence of carbonated minerals and Ca-modified silica gel, regardless of $MgSO_4$ content. However, a sufficient supply of sulfate ions induced the excessive formation of gypsum and lowered the CO_2 uptake levels after carbonation curing. These outcomes are anticipated to serve as fundamental information with regard to the integrity of carbonation curing of PC with CO_2 gas contaminated with magnesium and sulfate which would closely be influential to the safety of the final products.

1. Introduction

From its standardization in the early 1900 s, Portland cement (PC) has been acting as a guideline construction material for hydraulic binders, one which current behemoth relevant parties were founded upon [1]. Meanwhile, CO_2 has been regarded as an unfavorable/deteriorating factor for PC since it slowly degrades the hydration products of PC [2]. C-S-H, the main binder gel in PC, is well known to be decalcified to form silica gel upon extended exposure to CO_2, ultimately reducing the binding capability of the global matrix [3,4]. In addition, the ingress of CO_2 into PC lowers the pH levels of the pore solution which would pose threats to the stability of rebars embedded in concrete [5]. These CO_2-induced aspects are typically referred to as weathering carbonation [6].

On the other hand, the beneficial utilization of CO_2 by carbonation curing of PC in order to reduce the CO_2 footprint in producing PC-based materials and to geologically sequestrate CO_2 in the matrix is recently gaining significant attention as measures to deal with the global CO_2 crisis [2]. This strategy has been proposed five decades ago, yet the difficulties lay in the production of pure CO_2 gas and the negative perception on the use of CO_2 to PC-based materials remained obstacles to the widespread of the strategy [2]. Nevertheless, the intensive regulations imposed along the global CO_2 reduction campaign have re-examined the keen introduction of the carbonation curing technique, especially after the 2000 s [7]. Carbonation curing can rapidly enhance the mechanical strengths and improve durability performances of PC-based materials. In addition, the reaction of PC clinkers with low or none hydraulic properties (e.g., belite and mono-calcium silicate) is

☆ The following shorthand cement notations are used throughout the manuscript: S- SiO_2, C- CaO, A- Al_2O_3, $- SO_3, F- Fe_2O_3, M- MgO, T- TiO_2, $\overline{C}$- CO_2, N- Na_2O, K- K_2O, and H- H_2O.

* Corresponding authors at: School of Civil Enfineering, Chungbuk National University, 1 Chungdae-ro, Seowon-gu, Cheongju, Chungbuk 28644, Republic of Korea (Beomjoo Yang); Mineral Processing & Metallurgy Research Center, Resources Utilization Division, Korea Institute of Geoscience and Mineral Resources, 124 Gwahak-ro, Yuseong-gu, Daejeon 34132, Republic of Korea (G.M. Kim).
E-mail addresses: byang@chungbuk.ac.kr (B. Yang), k.gm@kigam.re.kr (G.M. Kim).

https://doi.org/10.1016/j.conbuildmat.2023.132806
Received 12 March 2023; Received in revised form 19 July 2023; Accepted 1 August 2023
0950-0618/© 2023 Elsevier Ltd. All rights reserved.

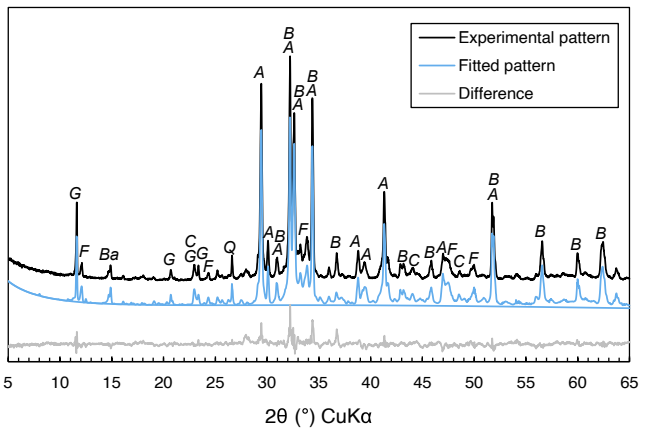

Fig. 1. X-ray diffractogram of the Portland cement used in this study. The annotations indicate the followings: G- gypsum, F- brownmillerite, Ba- basanite, C- calcite, Q- quartz, A- alite, and B- larnite.

known to be highly promoted by carbonation curing [8]. During the carbonation curing process, the gaseous CO_2 does not act as a catalyst but as a reactant, forming the PC matrix different from the normally cured PC [7]. The carbonation curing of PC results in the presence of calcium carbonates and silica gel with several minor traces of C-S-H, aluminum hydroxide, and gypsum [7,9].

The ultimate goal of carbonation curing aims at using CO_2 contained in the exhaust gas generated from industrial sectors in a beneficial way [10]. In general, exhaust gas can contain sulfate ions as well as CO_2. The sulfate attack on PC-based materials causes a major deterioration, which can influence the long-term durability of the structures [11–13]. The mechanism of sulfate attack on PC-based materials is highly relevant to cations accommodating sulfate ions and pore characteristics, binder chemistry, and aggregate type of the structures [14–16].

Meanwhile, the presence of Mg that is initially included in a cementitious matrix could affect the formation kinetics of calcium carbonates. The control over the content of Mg ions could affect the nucleation and structural characteristics of calcium carbonate polymorphs [17]. Zhang and Panesar [18] reported that Mg could be incorporated in calcite during carbonation of cement paste up to 30 mol %, and the coexistence of nesquehonite ($MgCO_3{\cdot}3H_2O$) in the matrix contributed to the formation of highly stable magnesium calcite. On the other hand, the conditions in which magnesium and sulfate ions exist simultaneously correspond to a harsh environment related to the durability of PC-based materials. Most commonly investigated, the $MgSO_4$ attack on PC induces the formation of $Mg(OH)_2$ and $CaSO_4$ layers onto the hydration products, thereby forming expansive ettringite and exhausting Ca from C-S-H [19,20]. Furthermore, $MgSO_4$ is well postulated to interact with most of the PC compounds, including clinkers, hence deteriorating the matrix, with final resultants of gypsum and ettringite [21,22]. In addition to the cracking and expansion phenomenon induced by the ingress of $MgSO_4$ to PC-based materials, loss of adhesion and bond strength between binder gel due to the conversion of C-S-H to M−S−H are primary features of $MgSO_4$ attack [23]. Against this background, understanding the coupled effects of magnesium and sulfate ions on PC under the carbonation curing condition is necessary. Earlier works [24–26] have identified the simultaneous sulfate attack on the PC-based materials exposed to extremely high CO_2 concentrations to simulate the wellbore or saline environments, all of which are clearly different from the carbonation curing conditions.

In this regard, this study intends to fill the knowledge gaps of research scope that occurred in-between earlier works at a microscopic level. The present study focuses on the alterations in the reaction properties of PC against coupled deteriorations of magnesium and sulfate upon carbonation curing. Specifically, physical and chemical changes happened during the carbonation curing in the presence of $MgSO_4$ were studied. The test outcomes reported in this study can serve as a fundamental guideline with regard to the integrity of carbonation curing of PC-based materials with CO_2 gas contaminated with magnesium and/or sulfate which would closely be related to the safety of the final products.

2. Experimental program

2.1. Raw materials

Ordinary PC (Hanil Cement Co. Ltd., in Korea) was used as a binder material. The XRD pattern and mineral composition of the raw PC is shown in Fig. 1. Note that the mineral composition of the raw PC was obtained from the Rietveld calculation of the XRD pattern, and was

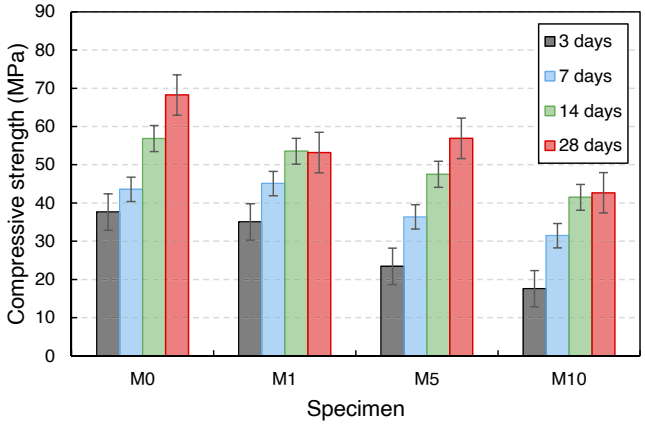

Fig. 2. Compressive strength development of the samples.

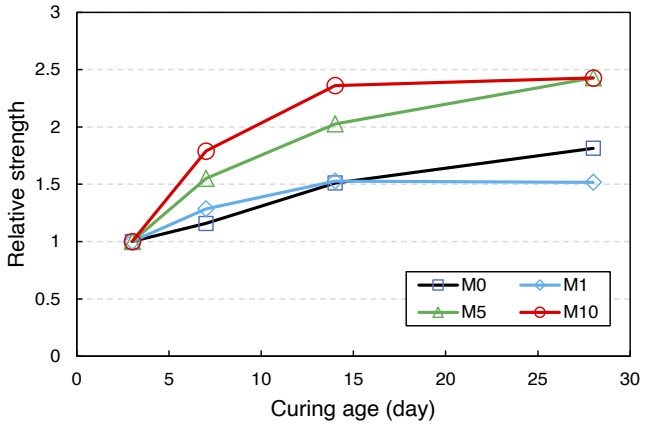

Fig. 3. Relative compressive strength development of the samples with respect to their strength at 3 days of curing.

Table 1
Mix proportion of the samples.

Mineral	C_3S	C_2S	$C\overline{C}$	C_4AF	$C\${\cdot}2H$	C_3A	$C\${\cdot}0.5H$	S	M
Content (wt.%)	49.2	16.3	9.5	8.3	6.1	5.1	2.7	1.4	1.3

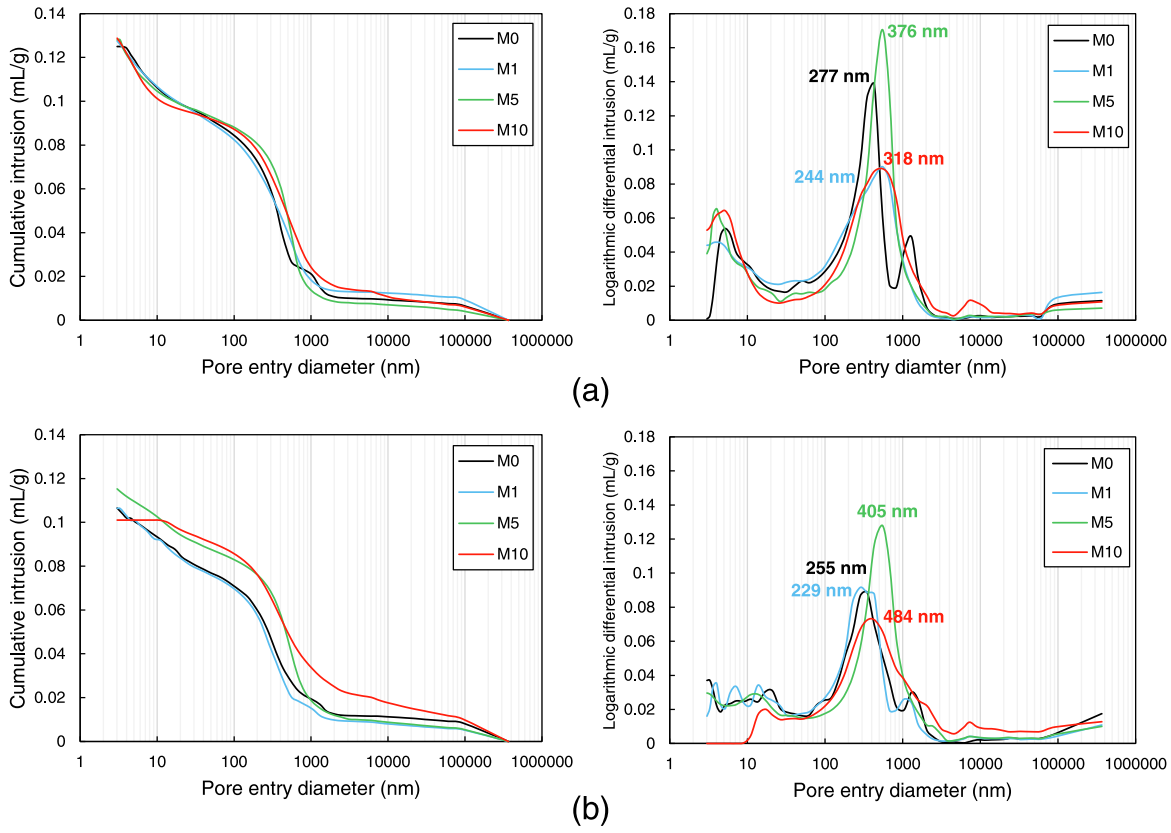

Fig. 4. Mercury intrusion curves of the samples at (a) 3 and (b) 28 days of curing.

listed in Table 1. The analytical-reagent grade anhydrous magnesium sulfate ($MgSO_4$, Sigma Aldrich, purity ≈ 99.5 %) was used to vary the conditions of Mg^{2+} and SO_4^{2-} ions in a cementitious matrix.

2.2. Mixture procedure and curing condition

Table 2 showed mix proportion of PC pastes with $MgSO_4$. A total of four types of samples were fabricated in the present study. The content of $MgSO_4$ varied from 0 % to 10 % of the weight of cement. Water to cement ratio was fixed at 0.4. The mixing procedure was as follows. Dry materials (selected from PC and $MgSO_4$ powders) were mixed for 1 min and water was added to the materials. The mixture was additionally mixed for 3 min and was cast into 50 mm cubic molds for compressive strength tests. The samples for the analytical tests to be introduced below were cast into 25 mm cubic molds. All the samples were placed in a carbonation chamber with a concentration of 10 % immediately after casting. The samples were demouled after 24 hrs and exposed to the identical carbonation condition until designated periods. The relative humidity during the carbonation was fixed at 60 %. It should be noted that the whole of the sample with a size of 25 mm was pulverized by sequentially using a jaw crusher and a cup mill after carbonation with a designated period. The samples before pulverization were immersed in anhydrous ethanol and put into a vacuum chamber to prevent an unexpected reaction. The vacuum process persisted until the anhydrous ethanol was fully evaporated. The use of the sample with the size (25 mm), and the whole pulverization was employed to minimize the effect of sample size on analytical tests after carbonation.

2.3. Characterization details

The samples underwent various investigating tools for the characterization upon carbonation curing. The compressive strength of the samples was carried out according to ASTM C109. The Universal Testing Machine (RT-M−003−30PC, Ramt Co., Ltd.) was used for the tests. The pore characteristics of the samples were investigated by a mercury intrusion porosimetry (MIP, AutoporeIV, Micromeritics Instrument Corporation) test. The maximum intrusion pressure, surface tension, and contact angle were 414 MPa, 0.485 N/m and 130°, respectively. The XRD test (D-MAX2500-PC manufactured by Rigaku) of samples was performed with CuKα radiation at 40 kV and 200 mA. The scanning range was from 5° to 65° with a scan step 0.02°/min. The heating rate in TGA tests (MaxRes TGA manufactured by Mettler-Toledo) was fixed at 10 °C/ min. N_2 gas was used to avoid sample oxidization. The TGA test results were processed using the tangential method from the DTG curves and were normalized to 100 g of PC. The solid-state ^{27}Al MAS NMR spectra of the samples were obtained using a 9.4 T Bruker AVANCE III HD instrument (Bruker Corporation, Billerica, MA, USA). 104.3 MHz transmitter frequency and a 4 mm MAS BB/BB probe were used. Thermodynamic modeling was performed using a software GEM-Selektor v3.3 with the aid of the database of CEMDATA18. The degree of hydration of clinkers was used to calculate the phase assemblages of the samples. The degree of hydration of clinkers (C_3S, C_2S, C_3A, and C_4AF) was described as a function of hydration time using the Rietveld calculation and Parrot Killoh's hydration model [27] by refining the equation parameters to match the experimental data. These parameters enabled the calculation of phase composition at specific time intervals, including up to 1000 days, thereby providing information on the evolution of the phase assemblage over an extended duration.

3. Results and discussion

3.1. Compressive strength

The compressive strength development of the samples is shown in

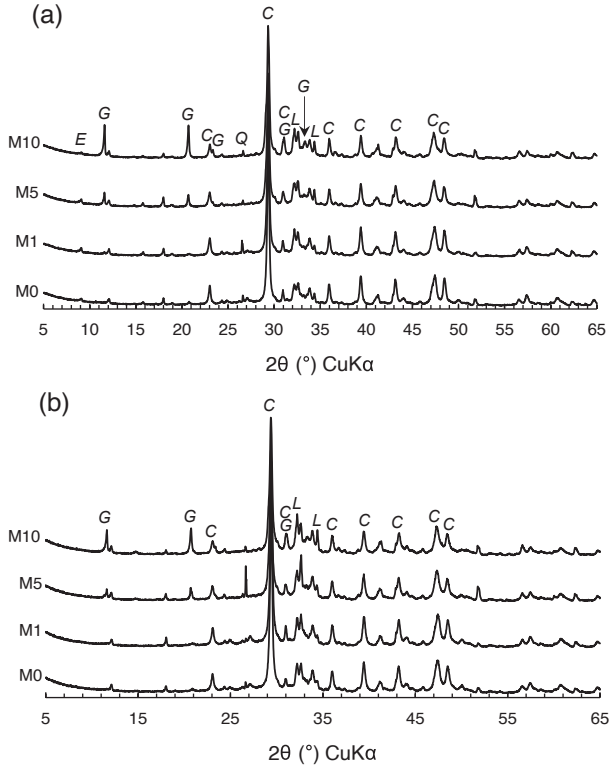

Fig. 5. X-ray diffractogram of the samples at (a) 3 and (b) 28 days of curing. The annotations indicate the following: E- ettringite, G- gypsum, C- calcite, L- larnite.

Fig. 2. The compressive strength values of the samples were greatly varied either by $MgSO_4$ content or by the progress of carbonation curing. In particular, the incorporation of $MgSO_4$ was found to have a detrimental influence on the strength development at an early stage. The compressive strength value of the M5 and M10 samples at 3 days of curing was 62.3% and 46.7% as compared to that of M0 sample, respectively, while the compressive strength value of the M1 sample was slightly lowered in comparison with that of M0 sample. This phenomenon indicates that the reduction in the strength development is closely related to what hydration products the dissolved $MgSO_4$ was engaged to interact with in the PC matrix. In addition, in what form and how these products existed as components in the PC matrix could have affected the strength reduction. Earlier works [28–30] demonstrated that the incorporated Mg cations in cementitious materials can result in the formation of excessive brucite, which consumes a large amount of free water present in the pore solution, hindering the hydration of PC clinkers. In addition, the formation of brucite is well postulated to induce expansion and volume instability phenomena in the PC-based materials [30–32], possibly degrading the strength developments in the samples with $MgSO_4$. Other than this aspect, the dilution effect induced by the reduction in the unit PC content may be responsible for the reduction in the compressive strength in the samples with $MgSO_4$. The compressive strength values of all samples tended to increase by the carbonation curing regardless of the $MgSO_4$ contents. The increase in the mechanical strength of the PC-based materials upon carbonation curing has been constantly reported in the relevant works [33–36] due to the accelerated reaction of clinkers. The carbonation reaction of clinkers typically yields C-S-H and calcium carbonates (Eqs. (1) and (2)) which enhances the mechanical and durability properties [36], yet further intensive carbonation can lead to the entire decalcification of the C-S-H [37–39].

$$C_3S + (3\text{-}x)CO_2 + yH_2O \rightarrow C_xSH_y + (3\text{-}x)CaCO_3 \quad (1)$$

$$C_2S + (2\text{-}x)CO_2 + yH_2O \rightarrow C_xSH_y + (2\text{-}x)CaCO_3 \quad (2)$$

The compressive strength levels of the samples progressively enhanced by carbonation curing, reaching the highest level of 68.3 MPa in the M0 sample at 28 days of curing. Meanwhile, the compressive strength value of the M1 and M5 samples at 28 days of curing was similar, and the M10 sample showed the lowest value of 42.7 MPa at 28 days of curing.

The relative compressive strength development of the samples with respect to their strength at 3 days of curing is shown in Fig. 3. The relative development in the compressive strength values of the samples can allow one to clearly observe the enhancement effect by the carbonation curing. The M0 and M1 samples showed lower and slower improvement in the compressive strength by carbonation curing than other samples. On the other hand, the M5 and M10 samples exhibited a general strength enhancement by carbonation curing, especially in the early stage of curing. The carbonation curing promoted a rapid development in the compressive strength in the M10 sample until 14 days of curing, yet there was no noticeable strength improvement afterward. The M10 sample showed the highest strength enhancement rate of 242% at 28 days of curing.

3.2. MIP

Mercury intrusion curves of the samples is shown in Fig. 4. The pore size distribution of the samples on the right in Fig. 4 indicates that the median pore diameter of the samples in which the trend of the values fairly followed the compressive strength results. The pore distribution outcomes of the samples at 3 days of curing indicate that the pore symptoms can be categorized into three regions. The first pore region was described at pore entry diameters of 1–10 nm. This pore region was occupied by the pores with regard to the presence of gel pores [36,40], particularly originated by the C-S-H in this work. The second pore region was characterized at pore entry diameters of 100–1000 nm which can be assigned to the large capillary pore region [41], and this region typically contained the median pore diameter. The center of the pore population peak in this region was slightly shifted toward the high pore diameter by the incorporation of $MgSO_4$. The last pore region was found at pore entry diameters larger than 1000 nm, typically known as the mesopore region [41]. The M10 sample particularly showed pore population in this region, all of which can possibly be associated with the presence of entrapped air or unhydrated clinkers [36]. The pores present in this region adversely affect the durability of PC-based materials and are believed to play a vital role in the low early strength development of the M10 sample. The median pore diameter of the samples was not vastly altered as carbonation proceeded. It is interesting to note that the formation of gel pores in the M10 sample was not recorded at 28 days of curing, indirectly meaning that the main binder gel was fully decalcified by carbonation. Other than this, all samples showed a broad range of pore symptoms at pore diameters of 10–3000 nm which signifies the presence of the amorphous Ca-modified silica gel formed by the partial or full decalcification of C-S-H (Eq. (3)) [40,42].

$$C_xS_yH_z + {}_xCO_2 \rightarrow xCaCO_3 + ySHt + (2\text{-}yt)H \quad (3)$$

In addition, the pore diameters at 10–200 nm were abundantly reported to display the nano-packing effect by calcite formation [36,42]. The porosity value of the M0, M1, M5, and M10 samples at 3 days of curing was 22.4%, 23.8%, 23.8%, and 20.9%, respectively, and that at 28 days of curing was 21.4%, 20.7%, 23.2%, and 19.9%, respectively, which is in close agreement with the compressive strength test results.

3.3. XRD

The XRD patterns of the samples is shown in Fig. 5. The peaks of ettringite were found in the samples containing $MgSO_4$ at 3 days of curing. Furthermore, increasing $MgSO_4$ content led to the increase of

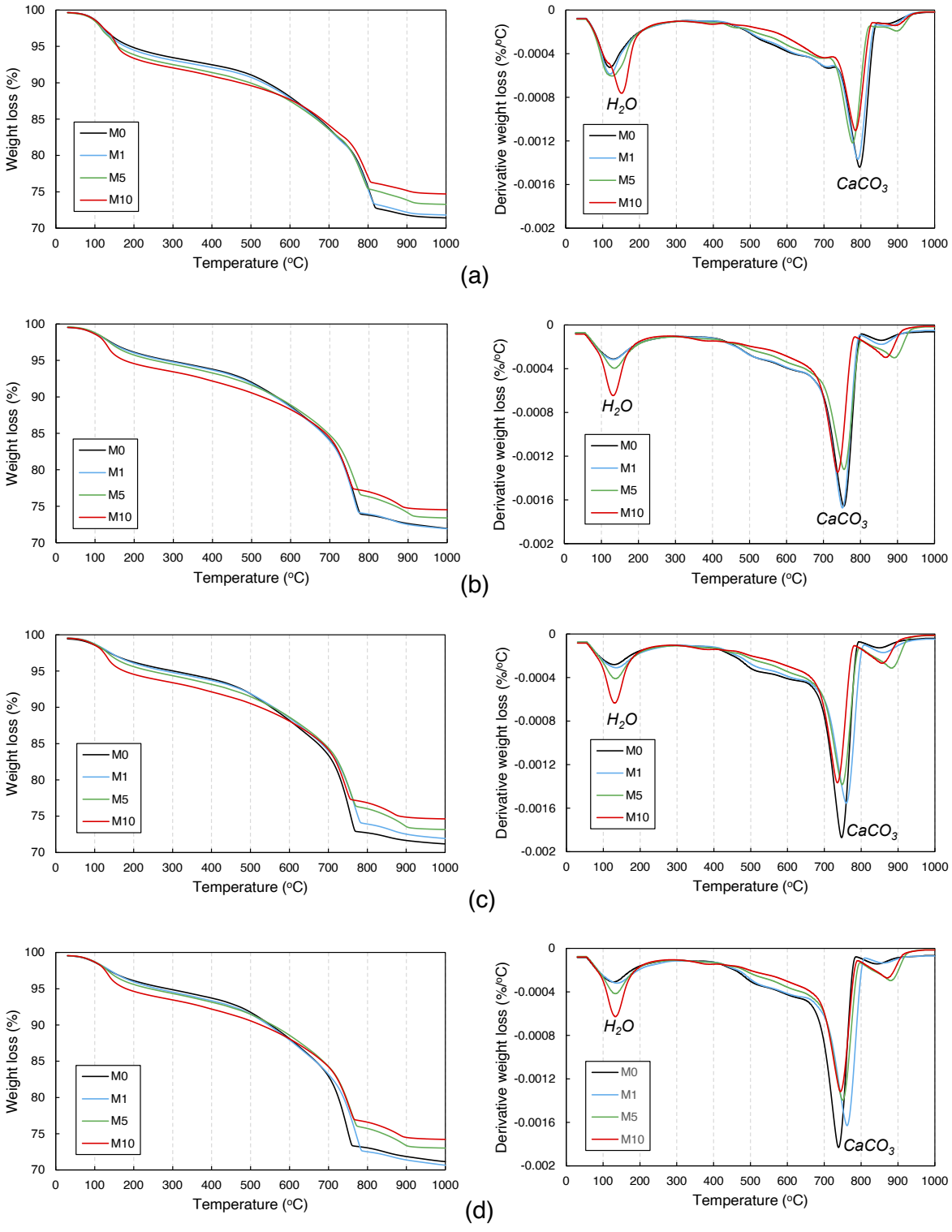

Fig. 6. Thermogravimetry curve of the samples at (a) 3, (b) 7, (c) 14, and (d) 28 days of curing.

peak intensity of gypsum which was not observable on the pattern of the M0 sample. The presence of gypsum in the samples containing $MgSO_4$ can be explained by a couple of facts: (1) carbonation of ettringite that was excessively formed at the very first moment of hydration by an internal SO_4^{2-} supply (Eq. (4) [43]); and (2) interaction of remnant SO_4^{2-} present in the pore solution with free Ca^{2+}.

$$C_6A\,\overline{S}H_{32} + 3CO_2 \rightarrow 3CaCO_3 + AH_3 + 3C\overline{S}\,H2 + 23H \quad (4)$$

Carbonation of hydration products exhibited peaks of calcite in all samples, while peaks of portlandite were not detected, indicating that a high degree of carbonation of the internal matrix has been reached within 3 days of carbonation. The unhydrated clinkers were found on the patterns of the samples by the traces of larnite. The XRD patterns of the samples at 28 days of curing showed a similar aspect to those at 3 days of curing, yet the peaks of ettringite were found to be fully vanished, meaning that the full carbonation of ettringite was achieved in the

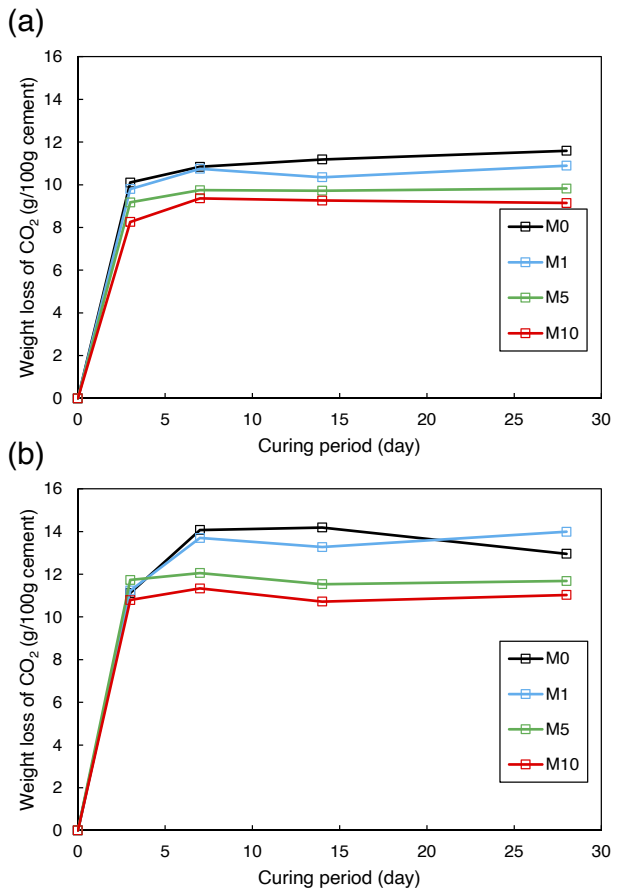

Fig. 7. Weight loss occurred in the temperature region of (a) 500–700 °C and (b) 700–800 °C in the samples as calculated from the data obtained by the thermogravimetry analysis.

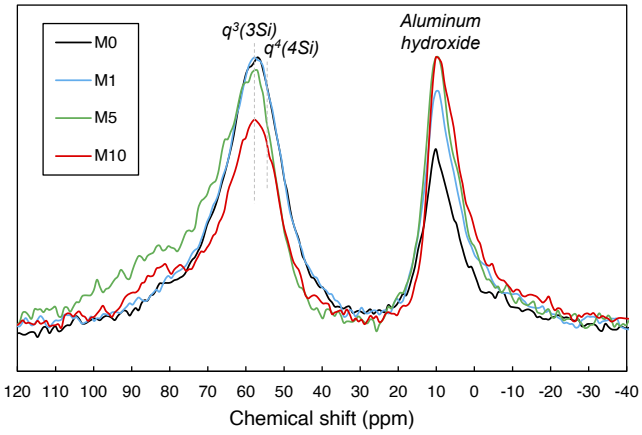

Fig. 8. Solid-state ^{27}Al MAS NMR spectroscopy of the samples at 28 days of curing.

samples. Carbonation curing did not vary the combinations of reaction products.

3.4. TGA

TGA curves of the samples are shown in Fig. 6. The samples featured three weight losses in the curves regardless of curing age: (1) evaporation of free water or weakly bound water in-between hydrates at 100–150 °C [39]; (2) broad weight loss at 500–700 °C [4]; and (3) decarbonation of calcite at 700–800 °C [44]. The weight loss occurred at 500–700 °C can be regarded to contain the decarbonation of unstable carbonates such as amorphous calcium carbonates, vaterite, and aragonite [4]. The two weight loss shoulders were identified at around 100—150 °C in the TGA curve of the samples at 3 days of curing, i.e., approximately at 100 °C and 140 °C. The weight loss found at 140 °C became clear as the $MgSO_4$ content increased, meaning that this weight loss was possibly associated with the dehydration of gypsum. However, the weight loss at 100 °C did not notably vary with the $MgSO_4$ content, thus can potentially be C-S-H particularly with a low Ca/Si ratio due to carbonation [42,45]. The two weight loss shoulders appeared at a temperature region of 100–150 °C became combined into one upon carbonation, and intensity increased with an increase of $MgSO_4$ content, hence can be assigned to the dominant weight loss associated with the dehydration of gypsum. The broad weight loss at 500–700 °C tended to decrease as the $MgSO_4$ content increased. This observation suggests two possible aspects. The formation of $MgCO_3$ from the incorporated $MgSO_4$ is not anticipated since the thermal decomposition temperature of the $MgCO_3$ is known to be happen approximately at 550 °C, however, increasing $MgSO_4$ content rather decreased the weight loss in this temperature region [46,47]. The other aspect is that the incorporation of $MgSO_4$ hindered the formation of unstable carbonates. In other words, it can be said that the calcite formation was preferred upon carbonation in the samples containing $MgSO_4$ which in turn contributed to the high compressive strength enhancement in these samples by pore packing effect by the calcite formation. The weight loss occurred in the temperature regions of calcium carbonates in the samples as calculated from the data obtained by the TGA results is summarized in Fig. 7. Note that these values were calibrated by the weight loss of CO_2 (g) per 100 g of PC.

3.5. ^{27}Al NMR

A number of Al nuclei were probed to quantitatively identify the alterations occurred in a specific Al site. Solid-state ^{27}Al MAS NMR spectroscopy of the samples at 28 days of curing is shown in Fig. 8. The samples commonly exhibited two spectral features of tetrahedrally and octahedrally coordinated Al sites at 90–50 ppm and 20-–10 ppm, respectively [48,49]. In the octahedrally coordinated Al region, a signal at 10 ppm was resonated in all samples. This resonance is deemed to designate aluminum hydroxide considering the earlier outcomes (XRD and TGA) and curing age. The intensity of resonance corresponding to aluminum hydroxide increased with an increase of $MgSO_4$ content. The increase in the resonance of aluminum hydroxide was due to the carbonation of ettringite which was further promoted by the incorporation of $MgSO_4$ in the samples (Eq. (4)). Other than this, the tetrahedrally coordinated Al region mainly contained q^3(3Si) and q^4(4Si) sites at 62 ppm and 58 ppm, respectively [50,51]. The q^3(3Si) and q^4(4Si) sites indicate the Al framework with a high degree of Al cross-linkage, formed by the carbonation of a system containing C-(A)-S-H [50,51]. Notable resonances of q^2 sites were not observable on the spectra, signifying that a considerable degree of carbonation has progressed to the binder gel [3,4]. The incorporated $MgSO_4$ reduced the intensity of resonances in the tetrahedrally coordinate Al sites; that is, the Al population in the samples preferred to contribute to the formation of aluminum hydroxide, formed by the carbonation of ettringite, rather than to the formation of highly crosslinked Al frameworks. Overall, PC-based systems with a high amount of SO_4^{2-} can hinder the substitution of Al in the C-S-H and the formation of resulting Al frameworks upon carbonation curing.

3.6. Thermodynamic modeling

The reaction degrees of PC clinkers were obtained by the Rietveld calculation of XRD patterns of the raw PC and samples at 3, 7, 14, and 28 days of curing. The Rietveld calculation of the XRD patterns was

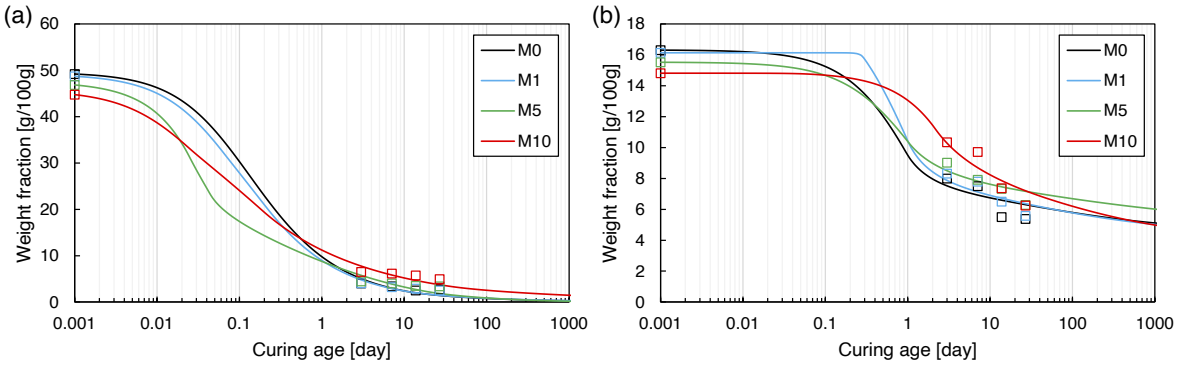

Fig. 9. Reaction degrees of (a) alite and (b) belite in the samples. Symbols and lines denote experimental and fitted results, respectively.

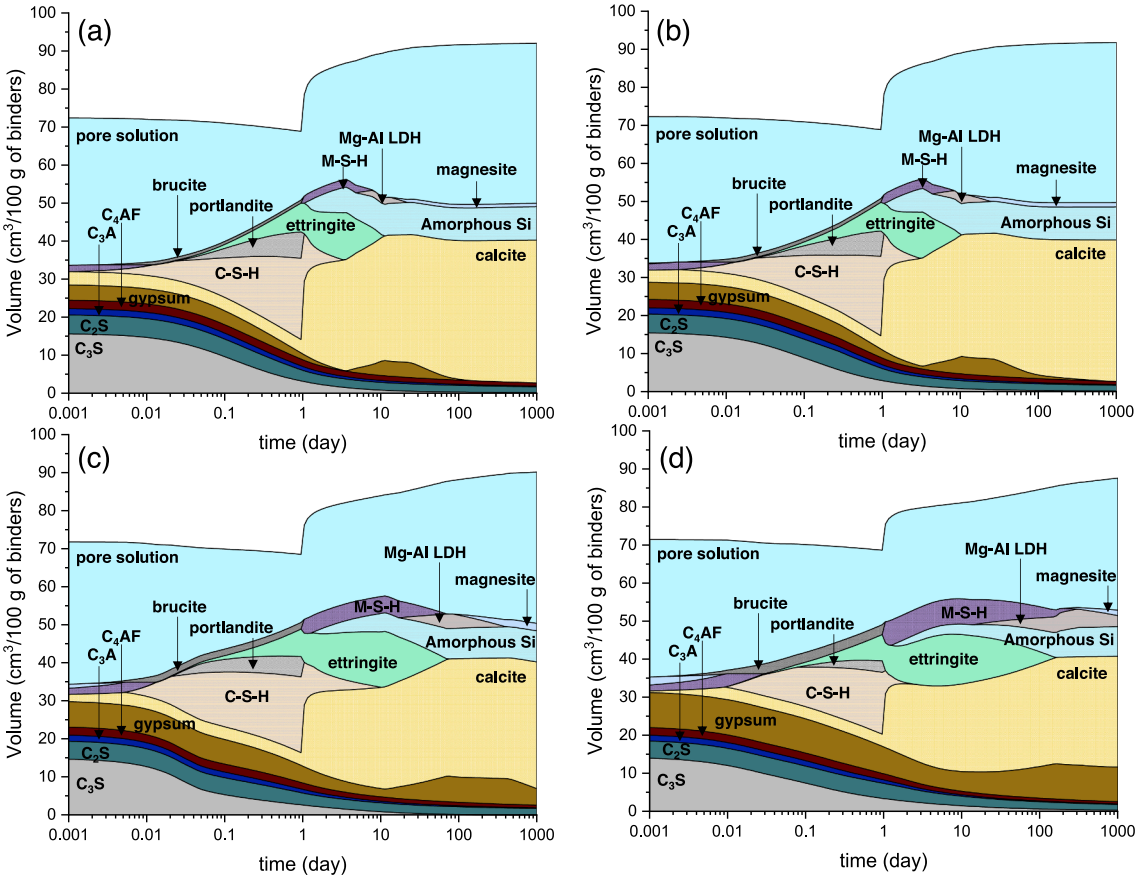

Fig. 10. Simulated phase assemblage and corresponding volume changes of the (a) M0, (b) M1, (c) M5, and (d) M10 samples upon interaction with carbonation curing.

carried out by an internal standard method with the corundum as an internal standard. The corundum was added to the designated samples at 10 wt%. Based on the quantification of the samples, the degree of reaction of alite and belite was described as a function of curing age using Parrot Killoh's hydration model [27]. The reaction degrees of alite and belite is shown in Fig. 9, and the obtained fitted model was used for modeling the phase assemblage in the samples.

Until the 1 day of hydration, the modeling results were calculated by the consumption of clinkers as provided by Fig. 9, but general hydration kinetics cannot be utilized since carbonation curing was additionally incorporated after 1 day of curing. In order to resolve this issue, the weight loss of CO_2 obtained by the TGA results was additionally added as the input data for thermodynamic modeling from the commencement of carbonation curing. As the TGA results of the samples were intermittent from 3 to 28 days of curing (i.e., 3, 7, 14, and 28 days of curing), the CO_2 uptake values between the testing days were fitted with a logarithmic relationship with curing age to construct the CO_2 input data.

Simulated phase assemblage and corresponding volume changes of the samples upon interaction with carbonation curing are shown in Fig. 10. The typical hydration aspect of the PC was provided in the results before 1 day of curing; the formation of portlandite, C-S-H, and ettringite with an exponential reduction of clinkers. The modeling indicated that the increase of $MgSO_4$ content leads to the increased formation of gypsum and ettringite. The amount of portlandite and C-S-H formed during the early hydration stage tended to decrease as the $MgSO_4$ content increased due mainly to the dilution of PC.

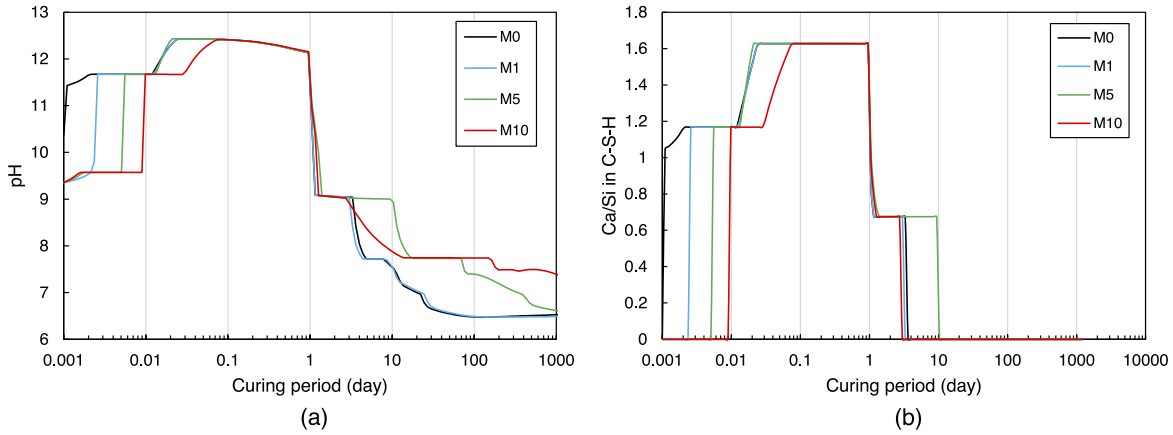

Fig. 11. Simulated (a) pH development and (b) Ca/Si in C-S-H of the samples.

With the commencement of carbonation curing, portlandite was the first phase to be carbonated immediately regardless of the $MgSO_4$ content and served as a chemical carbonation buffer, followed by the carbonation of C-S-H and ettringite. The modeling simulated that the carbonation of C-S-H resulted in the formation of M−S−H, with its content proportionally increased with an increase of $MgSO_4$ content, yet the formation of M−S−H could not be characterized by other test results. The decalcification of C-S-H also led to the presence of amorphous silica. It is interesting to note that the ettringite was simulated to be persisted in the M5 and M10 samples even after 28 days of curing, and gradually reduced afterward which is somewhat contradictory to the experimental test results provided in this study. The carbonation of hydration products eventually yielded $CaCO_3$ without distinguishing the carbonate species. The simulated amount of calcite was decreased as the $MgSO_4$ content increased because the CO_2 input data was acquired from the TGA where CO_2 uptake values were low in the samples with $MgSO_4$. Meanwhile, the volume of gypsum was increased during the carbonation due to the carbonation of ettringite.

Simulated pH development and Ca/Si in C-S-H of the samples are shown in Fig. 11. The initial pH development of the samples was delayed by the incorporation of $MgSO_4$, reflecting that the reaction kinetics of the clinkers were influenced by the $MgSO_4$. Nevertheless, $MgSO_4$ only affected the rate of pH development in the samples due to the fact that the maximum pH level reached in the samples was identical regardless of the $MgSO_4$ content. On the other hand, there was an instant reduction in the pH values upon carbonation curing, closely relevant to the rapid consumption of portlandite. A cascaded reduction in the pH levels was continuously found in the M0 and M1 samples after 1 day of curing, while this reduction was slightly lowered in the M5 and M10 samples due possibly to that the modeling simulated the excessive remnant ettringite even during the carbonation. In particular, the M5 and M10 samples maintained higher pH levels than other samples even after sufficient carbonation. The large amount of $CaSO_4$ content persisted in these samples was responsible for the high pH levels at the terminal stage. The Ca/Si in C-S-H of the samples followed the similar trend to the pH development of the samples due to the slow formation of C-S-H in the matrix. The maximum Ca/Si level in C-S-H reached was identical regardless of the $MgSO_4$ content, followed by a rapid decrease in the level upon carbonation curing, mainly associated with the elimination of Ca in the C-S-H by the decalcification process. The Ca/Si level in C-S-H of the samples quickly headed toward 0 in the samples, thereby producing amorphous Si. The moment of full decalcification of C-S-H was analogous in the samples except for the M5 sample. Note that the simulation results presented in Fig. 11 can provide insight on the evolution of pH values and Ca/Si in C-S-H in the samples beyond the limited testing timeframe.

4. Conclusion

The present study focused on the alterations in the reaction properties of PC against coupled deteriorations of magnesium and sulfate upon carbonation curing. The physical and chemical aspects of the samples containing various levels of $MgSO_4$ under the carbonation curing of 27 days were evaluated. The following conclusions were made based on the results obtained in this study.

(1) The incorporation of $MgSO_4$ reduced the compressive strength of the samples. However, the strength was vastly enhanced by carbonation curing.
(2) The samples contained carbonated minerals with traces of Ca-modified silica gel after carbonation curing regardless of $MgSO_4$ content.
(3) The promoted formation of ettringite due to the incorporation of $MgSO_4$ resulted in the presence of gypsum after the carbonation curing.
(4) The incorporation of $MgSO_4$ lowered the CO_2 uptake levels and contributed to the formation of aluminum hydroxide rather than that of a highly crosslinked Al framework after the carbonation curing.
(5) The modeling results predicted that the $MgSO_4$ did not influence the maximum pH and Ca/Si in C-S-H reached. Even so, the rate of pH and Ca/Si development were delayed by the incorporation of $MgSO_4$ due to the reduced reactivity of PC clinkers.

CRediT authorship contribution statement

Joonho Seo: Conceptualization, Methodology, Writing – original draft, Project administration, Funding acquisition. **Naru Kim:** Formal analysis, Visualization. **Beomjoo Yang:** Validation, Investigation, Data curation, Supervision. **G.M. Kim:** Supervision, Writing – review & editing.

Declaration of Competing Interest

The authors declare that they have no known competing financial interests or personal relationships that could have appeared to influence the work reported in this paper.

Data availability

The authors do not have permission to share data.

Acknowledgments

This work was supported by Korea Institute of Energy Technology Evaluation and Planning(KETEP) grant funded by the Korea government (MOTIE)(20212010200080, In-situ carbonation technology development using CO_2 emissions from cement industry).

References

[1] K.L. Scrivener, R. Snellings, The rise of Portland cements. Elements, Int. Magaz. Mineral., Geochem. Petrol. 18 (5) (2022) 308–313.
[2] D. Zhang, Z. Ghouleh, Y. Shao, Review on carbonation curing of cement-based materials, J. CO2 Util. 21 (2017) 119–131.
[3] T. Gutberlet, H. Hilbig, R. Beddoe, Acid attack on hydrated cement—Effect of mineral acids on the degradation process, Cem. Concr. Res. 74 (2015) 35–43.
[4] J. Seo, S.M. Park, H.-K. Lee, Evolution of the binder gel in carbonation-cured Portland cement in an acidic medium, Cem. Concr. Res. 109 (2018) 81–89.
[5] G. Trabanelli, C. Monticelli, V. Grassi, A. Frignani, Electrochemical study on inhibitors of rebar corrosion in carbonated concrete, Cem. Concr. Res. 35 (9) (2005) 1804–1813.
[6] J. Gonzalez, C. Andrade, Effect of carbonation, chlorides and relative ambient humidity on the corrosion of galvanized rebars embedded in concrete, Br. Corros. J. 17 (1) (1982) 21–28.
[7] W. Ashraf, Carbonation of cement-based materials: Challenges and opportunities, Constr. Build. Mater. 120 (2016) 558–570.
[8] J.G. Jang, G.M. Kim, H.J. Kim, H.K. Lee, Review on recent advances in CO2 utilization and sequestration technologies in cement-based materials, Constr. Build. Mater. 127 (2016) 762–773.
[9] T. Nishikawa, K. Suzuki, S. Ito, K. Sato, T. Takebe, Decomposition of synthesized ettringite by carbonation, Cem. Concr. Res. 22 (1) (1992) 6–14.
[10] J. Liu, Y. Wang, Y. Li, J. Tian, X. You, Y. Mao, X. Hu, C. Shi, Carbonated concrete brick capturing carbon dioxide from cement kiln exhaust gas, Case Stud. Constr. Mater. 17 (2022) e01474.
[11] Marchand, J., I. Odler, and J.P. Skalny, *Sulfate attack on concrete*. 2001: CRC Press.
[12] N.M. Al-Akhras, Durability of metakaolin concrete to sulfate attack, Cem. Concr. Res. 36 (9) (2006) 1727–1734.
[13] E. Irassar, A. Di Maio, O. Batic, Sulfate attack on concrete with mineral admixtures, Cem. Concr. Res. 26 (1) (1996) 113–123.
[14] I. Ismail, S.A. Bernal, J.L. Provis, S. Hamdan, J.S.J. van Deventer, Microstructural changes in alkali activated fly ash/slag geopolymers with sulfate exposure, Mater. Struct. 46 (3) (2013) 361–373.
[15] E. Irassar, Sulfate attack on cementitious materials containing limestone filler—A review, Cem. Concr. Res. 39 (3) (2009) 241–254.
[16] D. Kanaan, A.M. Soliman, A.R. Suleiman, Zero-Cement Concrete Resistance to External Sulfate Attack: A Critical Review and Future Needs, Sustainability 14 (4) (2022) 2078.
[17] J. Kawano, S. Maeda, T. Nagai, The effect of Mg 2+ incorporation on the structure of calcium carbonate clusters: investigation by the anharmonic downward distortion following method, PCCP 18 (4) (2016) 2690–2698.
[18] R. Zhang, D.K. Panesar, Investigation on Mg content in calcite when magnesium calcite and nesquehonite co-precipitate in hardened cement paste, Thermochim Acta 654 (2017) 203–215.
[19] D. Bonen, M.D. Cohen, Magnesium sulfate attack on portland cement paste-I. Microstructural analysis, Cem. Concr. Res. 22 (1) (1992) 169–180.
[20] D. Bonen, M.D. Cohen, Magnesium sulfate attack on portland cement paste—II. Chemical and mineralogical analyses, Cem. Concr. Res. 22 (4) (1992) 707–718.
[21] S. Thokchom, P. Ghosh, S. Ghosh, Performance of fly ash based geopolymer mortars in sulphate solution, J. Eng. Sci. Technol. Rev. 3 (1) (2010) 36–40.
[22] Z. Baščarević, M. Komljenović, Z. Miladinović, V. Nikolić, N. Marjanović, R. Petrović, Impact of sodium sulfate solution on mechanical properties and structure of fly ash based geopolymers, Mater. Struct. 48 (3) (2015) 683–697.
[23] P. Mehta, Sulfate attack on concrete–a critical review, Mater. Sci. Concr., IIIpp. (1992) 105.
[24] Q. Li, Y.M. Lim, Y.-S. Jun, Effects of sulfate during CO2 attack on Portland cement and their impacts on mechanical properties under geologic CO2 sequestration conditions, Environ. Sci. Tech. 49 (11) (2015) 7032–7041.
[25] S.J. Keller, Analyses of subsurface brines of Indiana, Indiana Geological & Water Survey, 1983.
[26] L. Zhang, D.A. Dzombak, D.V. Nakles, S.B. Hawthorne, D.J. Miller, B.G. Kutchko, C. L. Lopano, B.R. Strazisar, Characterization of pozzolan-amended wellbore cement exposed to CO2 and H2S gas mixtures under geologic carbon storage conditions, Int. J. Greenhouse Gas Control 19 (2013) 358–368.
[27] Parrot, L. *Prediction of cement hydration*. In: *Proceedings of the British Ceramic Society*. 1984.
[28] J. Seo, et al., Characterization of reactive MgO-modified calcium sulfoaluminate cements upon carbonation, Cem. Concr. Res. 146 (2021), 106484.
[29] Y. Yang, Y. Deng, X. Li, Uniaxial compression mechanical properties and fracture characteristics of brucite fiber reinforced cement-based composites, Compos. Struct. 212 (2019) 148–158.
[30] H. Lee, R.D. Cody, A.M. Cody, P.G. Spry, Observations on brucite formation and the role of brucite in Iowa highway concrete deterioration, Environ. Eng. Geosci. 8 (2) (2002) 137–145.
[31] M.R. Nokken, Expansion of MgO in cement pastes measured by different methods, ACI Mater. J. 107 (1) (2010) 80.
[32] Y.e. Qing, C. Huxing, W. Yuqing, W. Shangxian, L. Zonghan, Effect of MgO and gypsum content on long-term expansion of low heat Portland slag cement with slight expansion, Cem. Concr. Compos. 26 (4) (2004) 331–337.
[33] J.-H. Bae, et al., Evaluation of physicochemical properties and environmental impact of environmentally amicable Portland cement/metakaolin bricks exposed to humid or CO2 curing condition, J. Build. Eng. 47 (2022), 103831.
[34] J. Seo, I. Amr, S. Park, R. Bamagain, B. Fadhel, G. Kim, A. Hunaidy, H. Lee, CO2 uptake of carbonation-cured cement blended with ground volcanic ash, Materials 11 (11) (2018) 2187.
[35] S. Park, J. Seo, H.-K. Lee, Thermal evolution of hydrates in carbonation-cured Portland cement, Mater. Struct. 51 (2018) 1–8.
[36] J.G. Jang, H.-K. Lee, Microstructural densification and CO2 uptake promoted by the carbonation curing of belite-rich Portland cement, Cem. Concr. Res. 82 (2016) 50–57.
[37] R. Hameed, J. Seo, S. Park, I.T. Amr, H.K. Lee, Co2 uptake and physicochemical properties of carbonation-cured ternary blend portland cement–metakaolin–limestone pastes, Materials 13 (20) (2020) 4656.
[38] J. Seo, et al., Carbonation of calcium sulfoaluminate cement blended with blast furnace slag, Cem. Concr. Compos. 118 (2021), 103918.
[39] J. Seo, et al., Internal carbonation of belite-rich Portland cement: An in-depth observation at the interaction of the belite phase with sodium bicarbonate, J. Build. Eng. 44 (2021), 102907.
[40] T.A.B.J. Kropp, H. Hilsdorf, Formation of silica gel during carbonation of cementitious systems containing slag cements, Special Publication 114 (1989) 1413–1428.
[41] J.H. Seo, S.M. Park, B.J. Yang, J.G. Jang, Calcined oyster shell powder as an expansive additive in cement mortar, Materials 12 (8) (2019) 1322.
[42] J. Seo, et al., Microstructural evolution and carbonation behavior of lime-slag binary binders, Cem. Concr. Compos. 119 (2021), 104000.
[43] J. Seo, et al., Effect of the molar ratio of calcium sulfate over ye'elimite on the reaction of CSA cement/slag blends under an accelerated carbonation condition, J. Build. Eng. 46 (2022), 103785.
[44] J.G. Jang, H.J. Kim, S.M. Park, H.K. Lee, The influence of sodium hydrogen carbonate on the hydration of cement, Constr. Build. Mater. 94 (2015) 746–749.
[45] A. Nonat, The structure and stoichiometry of CSH, Cem. Concr. Res. 34 (9) (2004) 1521–1528.
[46] S.-B. Choi, N.-W. Kim, D.-K. Lee, H. Yu, Growth mechanism of cubic MgO granule via common ion effect, J. Nanosci. Nanotechnol. 13 (11) (2013) 7577–7580.
[47] D. Mahon, G. Claudio, P. Eames, An experimental study of the decomposition and carbonation of magnesium carbonate for medium temperature thermochemical energy storage, Energies 14 (5) (2021) 1316.
[48] S.M. Park, J. Jang, H.-K. Lee, Unlocking the role of MgO in the carbonation of alkali-activated slag cement, Inorg. Chem. Front. 5 (7) (2018) 1661–1670.
[49] N. Mobasher, S.A. Bernal, J.L. Provis, Structural evolution of an alkali sulfate activated slag cement, J. Nucl. Mater. 468 (2016) 97–104.
[50] D. Mueller, D. Hoebbel, W. Gessner, 27Al NMR studies of aluminosilicate solutions. Influences of the second coordination sphere on the shielding of aluminium, Chem. Phys. Lett. 84 (1) (1981) 25–29.
[51] Davidovits, J. *Chemistry of geopolymeric systems, terminology*. In: *Geopolymer*. 1999. Sn.